Supplement of Atmos. Chem. Phys., 26, 10331–10353, 2026
https://doi.org/10.5194/acp-26-10331-2026-supplement

Atmospheric Chemistry and Physics
Open Access
EGU

Supplement of

Contribution of free tropospheric aerosols to Arctic low-level cloud droplets formation and longwave radiative forcing

Roman Pohorsky et al.

Correspondence to: Roman Pohorsky (roman.pohorsky@epfl.ch) and Julia Schmale (julia.schmale@epfl.ch)

Supplemental information

Table S1 List of Helikite flights during the ARTofMELT campaign. Indicated take-off and landing times are in UTC. A cloud value of 0 indicates either a clear sky day or a cloud base higher than the maximum reached altitude of the Helikite during the flight. A value of 1 indicates that the Helikite sampled in a cloud but did not reach above cloud top. A value of 2 indicates that the Helikite went above the cloud top. The deployment of each instrument is listed in different columns, with 1 meaning the instrument was present and 0 not present. ST stands for SmartTether.

Flight	Date	Take off	Landing	Max altitude (m)	Cloud	ST	POPS	mSEMS	LOAC
1	2023-05-16	20:01:02	20:42:49	267	0	1	1	1	1
2	2023-05-17	11:23:33	13:45:48	441	0	1	1	1	1
3	2023-05-18	09:54:52	13:40:22	503	2	1	1	1	0
4	2023-05-18	14:47:00	19:02:06	482	0	1	1	1	0
5	2023-05-19	14:27:22	17:57:00	479	0	1	1	1	0
6	2023-05-23	11:51:05	14:24:48	368	1	1	1	1	0
7	2023-05-23	14:56:57	17:36:30	556	2	1	1	1	0
8	2023-05-29	10:46:24	12:10:36	246	0	0	1	1	1
9	2023-05-29	14:01:30	16:34:23	454	0	1	1	1	1
10	2023-06-02	10:09:48	12:12:31	443	0	1	1	1	1
11	2023-06-02	14:30:26	20:03:38	496	1	1	1	0	1
12	2023-06-03	14:24:57	14:45:26	205	1	1	1	1	0
13	2023-06-03	14:53:10	17:16:45	657	2	1	1	1	0
14	2023-06-04	13:47:38	16:27:19	560	2	1	1	1	0
15	2023-06-04	17:02:38	21:02:16	403	2	1	1	1	0
16	2023-06-06	14:14:00	20:26:32	547	0	1	1	0	1
17	2023-06-07	10:10:03	13:52:26	410	2	1	1	1	0
18	2023-06-07	14:31:06	17:35:44	481	2	1	1	1	0
19	2023-06-07	19:09:04	22:13:54	580	2	1	1	1	0
20	2023-06-09	09:31:50	11:39:02	533	0	1	1	1	0
21	2023-06-10	10:06:46	12:57:46	474	1	1	1	1	1
22	2023-06-10	13:41:48	16:50:50	466	2	1	1	1	1
23	2023-06-10	17:19:25	20:05:40	468	1	1	1	1	1

In addition, a single channel tricolor absorption photometer (STAP model 9406, Brechtel Manufacturing Inc., USA) measured aerosol light absorption coefficients at 450, 525 and 624 nm, an 8-channel filter sampler (FILT model 9401, Brechtel Manufacturing Inc., USA) collected aerosol particles on transmission electron microscopy copper grids and a filter sampler

(IcePuck, Handix, USA) collected aerosol particles on polycarbonate filters for INP analyses. The filter-sampling instruments were deployed on some flights, but their data are not presented here.

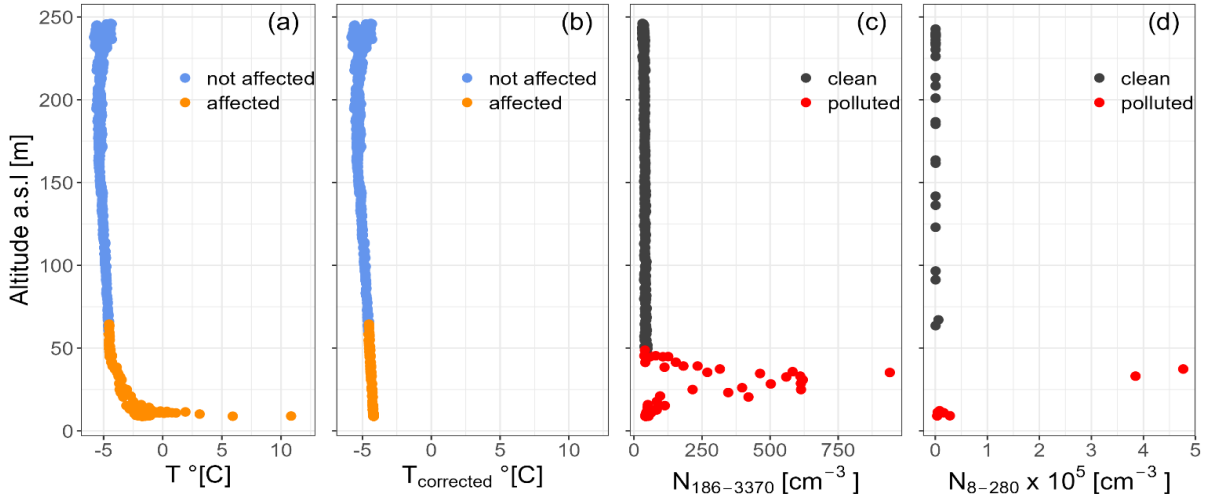

Figure S1 Example profiles from flight 8 on May 29, 2025 of (a) temperature, (b) corrected temperature, (c) $N_{186\text{-}3370}$ and (d) $N_{8\text{-}280}$. For temperature profiles, the color indicates temperature measurements affected by the ship's heat, which is corrected in (b). For aerosol profiles, the red dots correspond to the identified ship pollution.

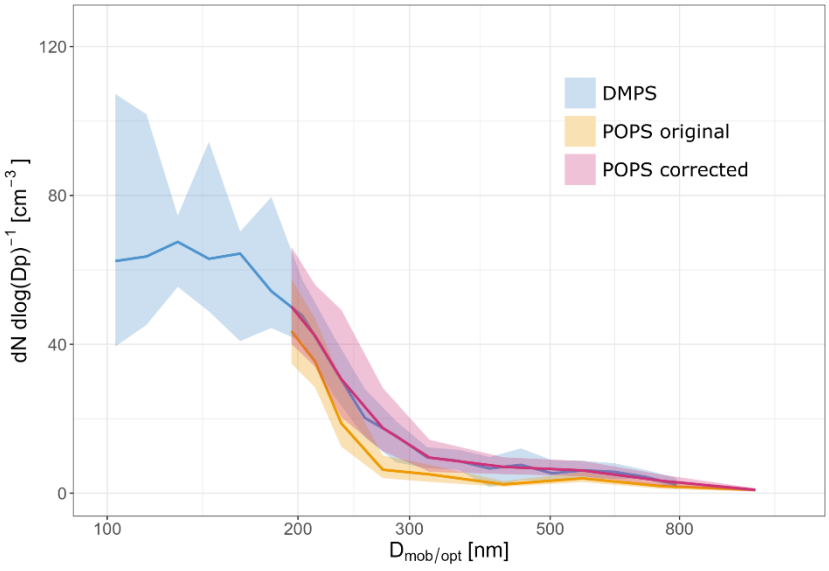

Figure S2 Size distribution measured with the DMPS and POPS during the ship-based intercomparison. The pink size distribution represents the corrected concentrations after the correction factors have been applied.

Table S2 Correction factors applied to the POPS original concentration values per bin.

POPS bin	Midpoint diameter (nm)	Multiplication factor
b3	195	1.15
b4	212	1.19
b5	234	1.63
b6	272	2.78
b7	322	1.89
b8	422	2.98
b9	561	1.53
b10	748	1.77
b11	1054	1
b12	1358	1
b13	1802	1
b14	2440	1
b15	3061	1

LOAC data validation

A quantitative comparison between the LOAC and a reference instrument (FM120, Droplet Measurement Technologies, USA) was performed during a side-by-side deployment at the end of the campaign covering two fog events (Fig. S3). The droplet concentrations measured by the two instruments were well correlated (adjusted R^2 = 0.83), indicating that the LOAC successfully captured temporal variations in cloud droplet number concentration. A linear regression yielded a slope of 0.74, suggesting that the LOAC systematically reported lower droplet concentrations than the FM120. Given the scatter in the comparison, the LOAC-derived droplet concentrations should be considered accurate within approximately 20–30 %.

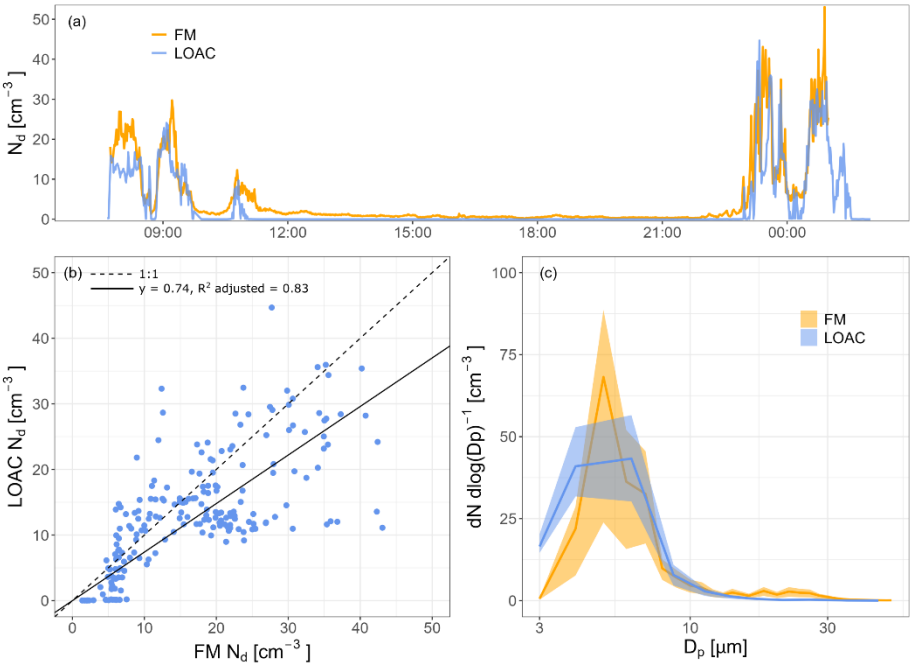

Figure S3 Intercomparison of the LOAC and Fog monitor between June 11 and June 12, 2023 on top of the aerosol-cloud laboratory on the fourth deck. (a) Total droplet number concentration measured by each instrument. (b) Scatterpot of droplet number concentrations (N_d) at a time resolution of 1 min for the LOAC and FM during two peak fog events between 07:45 and 09:40 on June 11 and 23:20 and 01:00 from June 11 to June 12. The dashed line represents the 1:1 line and the full line represents a liner regression with a slope of 0.74. (c) Average cloud droplet number size distributions measured by the LOAC and FM during the two fog events.

From the LOAC measurements, the liquid water content was calculated as:

$$LWC = \sum_{i=1}^{n} N_i \frac{4}{3} \pi \left(\frac{D_i}{2}\right)^3 \rho_w 10^{-6}, \quad (1)$$

where i represents the size bin and n the number of size bins. N_i is the droplet number concentration for bin i, D_i is the midpoint diameter of droplets in bin i (in µm), and ρ_w is the density of water (1 g cm^{-3}). The LWC is expressed in g m^{-3}.

The corresponding effective radius was calculated as

$$r_{eff} = \frac{\int_0^\infty r_i^3 n(r_i) dr}{\int_0^\infty r_i^2 n(r_i) dr}, \quad (2)$$

where r is the droplet radius associated with size bin i.

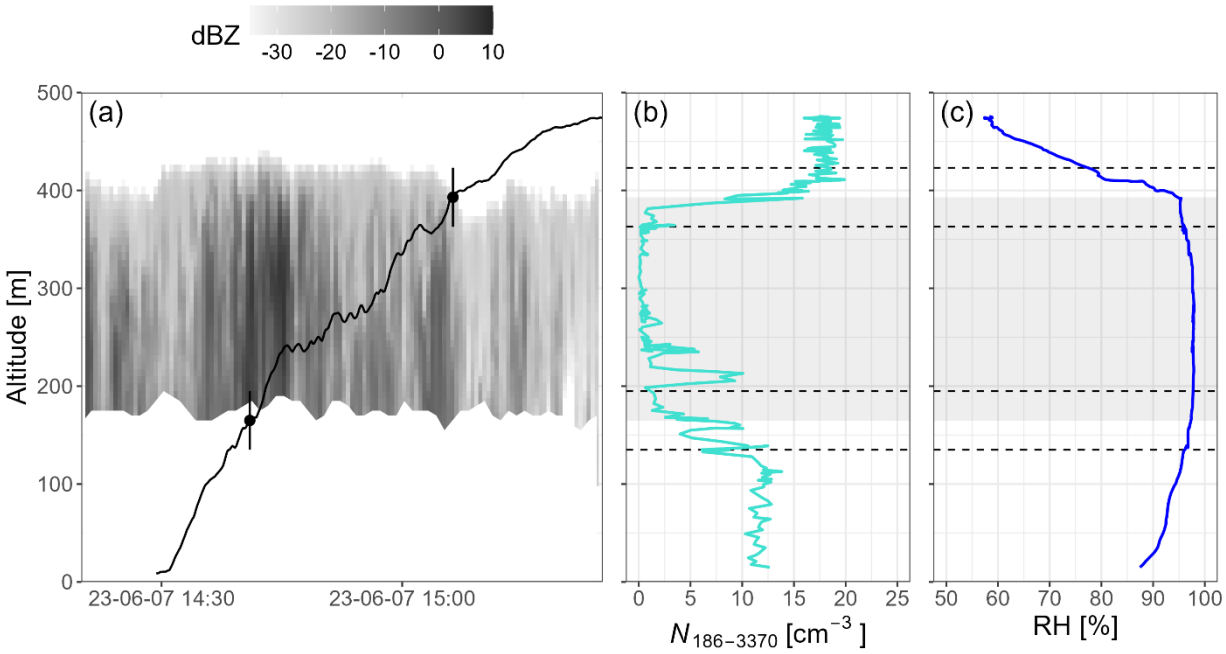

Figure S4 Example of cloud boundaries identification. On panel (a), grey filling indicates the cloud radar reflectivity and the trace represents the Helikite altitude. Panels (b) and (c) show vertical profiles of particle number concentration between 186 and 3370 nm and RH, respectively. The cloud boundaries represented by dots in (a) and grey shading in (b) and (c) were identified at 393 m a.m.s.l for the top and 165 m for the base. A ± 30 m uncertainty on the cloud boundaries is indicated by vertical error bars in (a) and horizontal dashed line in (b) and (c).

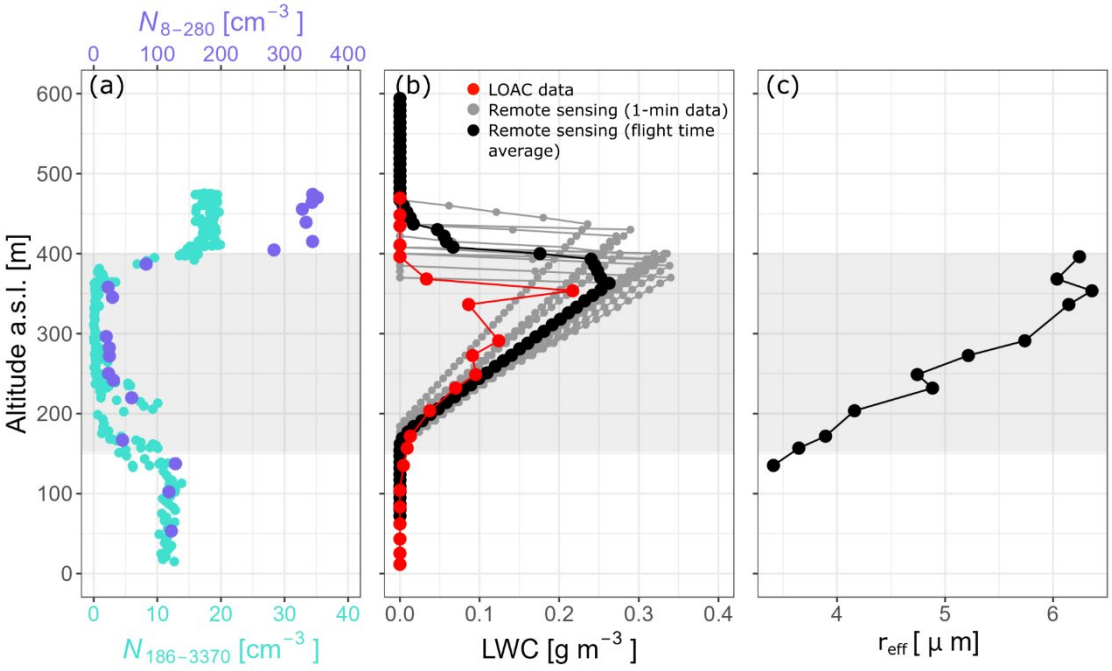

Figure S5 Vertical atmospheric profile between 14:40 and 15:07 UTC, on June 7th, 2023. Panel (a) represents the aerosol concentration profile for two size ranges, (b) represents the LWC measured by the LOAC (in red) and derived from the remote sensing measurements (grey = 1 minute time resolution, black = averaged over the profile duration), and (c) the droplet effective radius (r_{eff}) from the LOAC measurements.

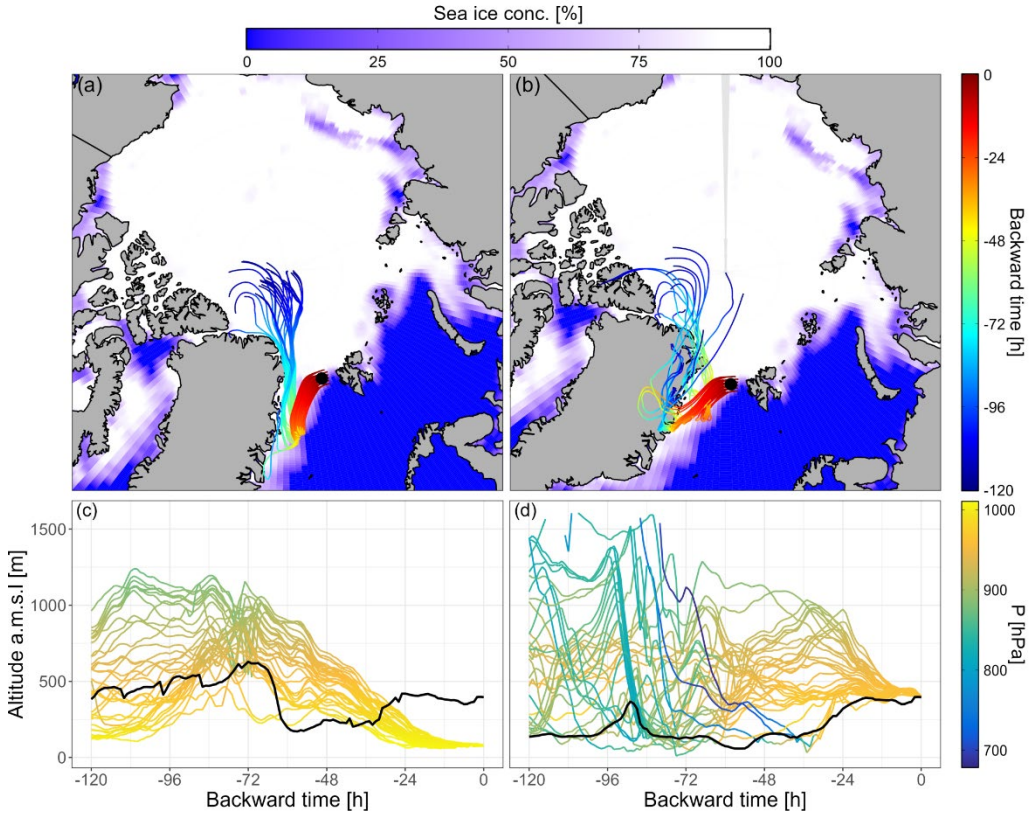

Figure S6 Five-day backtrajectory analysis of air masses arriving at the ship location on June 7th at 12:00 UTC. The 37 backtrajectories were calculated with the LAGRANTO model. (a) and (c) Trajectories arriving at the surface (1013 hPa). Panels (b) and (d) Trajectories arriving above the boundary layer (950 hPa). The top panels show the horizontal path of the air masses and the bottom panels show the vertical path. On the bottom panels, the average depth of the atmospheric boundary layer along the air mass path is shown (black line).

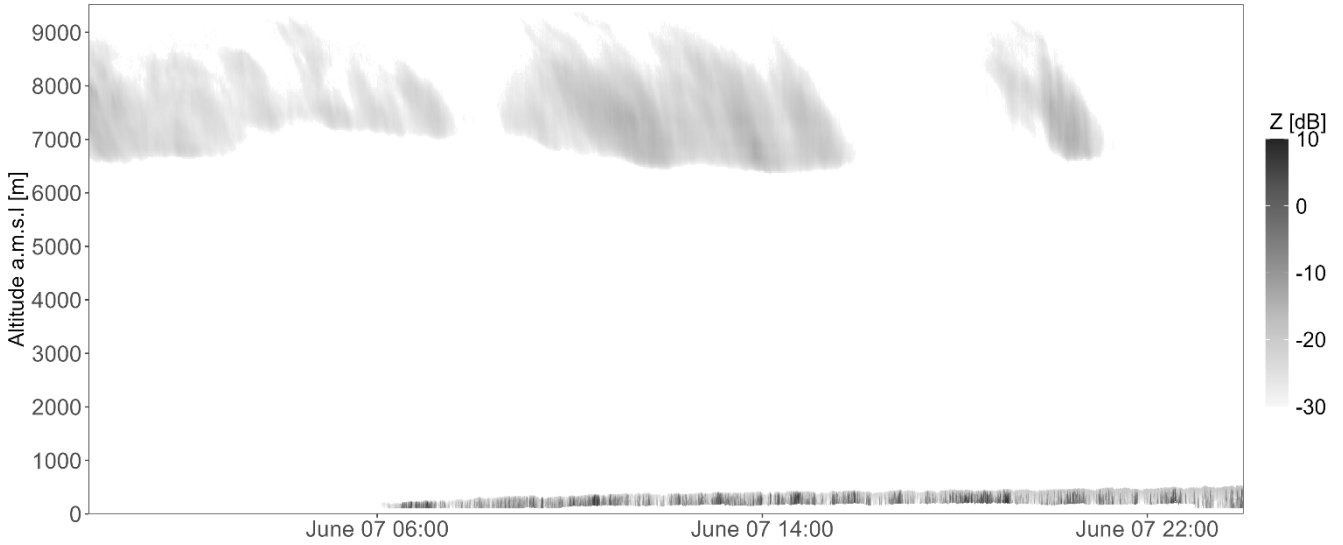

Figure S7 Time series of radar reflectivity, indicating the presence of clouds up to 10'000 m above sea level on June 7, 2023.

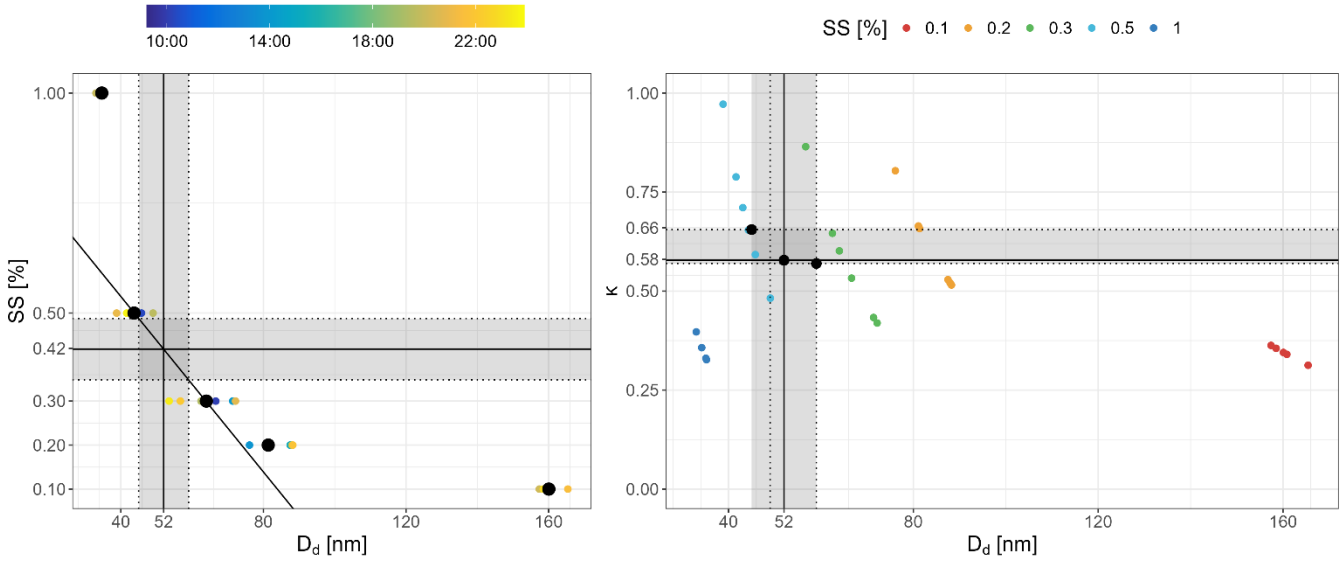

Figure S8 (a) Calculated critical activation diameters (D_d) for different supersaturation levels of the CCNC throughout the day on June 7, 2023. Black dots represent the daily average for each supersaturation. The black line represents a linear interpolation between two supersaturation levels, used to estimate the cloud's supersaturation for a D_d of 52 nm (i.e., measured Hoppel minimum). Grey shadings indicate uncertainty ranges corresponding to 10 % of the Hoppel minimum. (b) Calculated κ-values as a function of D_d and supersaturation. The black dots represent the best estimate and uncertainty range, highlighted by the grey shading.

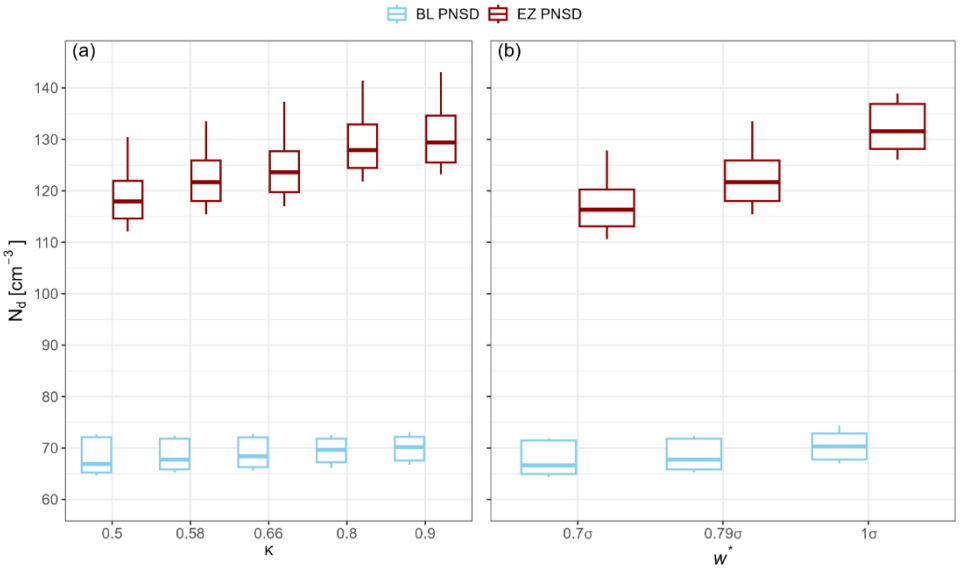

Figure S9 (a) Boxplot of droplet numbers from the aerosol activation parametrization using the boundary layer PNSD (blue) and entrainment zone PNSD (dark red) as inputs for different κ-values. (b) Parametrized maximum supersaturation with the two different PNSD inputs for different characteristic velocities. The boxplots represent the median and interquartile range, the whiskers' length equals to 1.5 times the interquartile range.

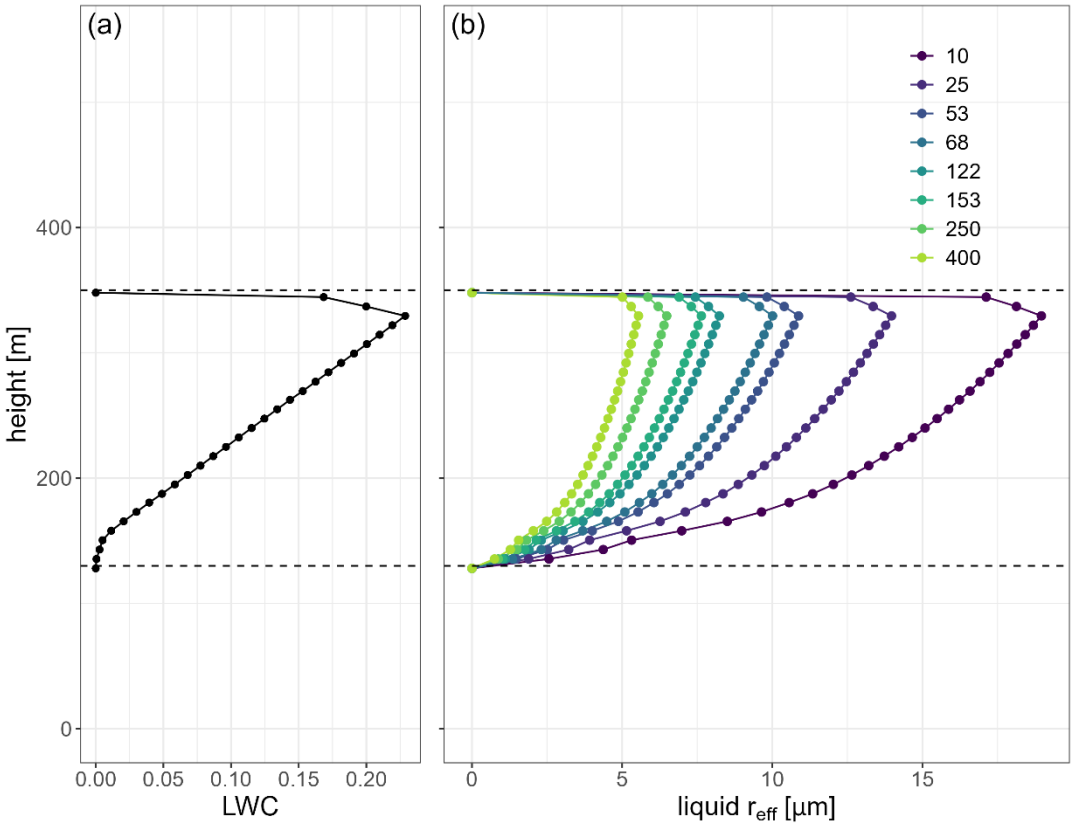

Figure S10 Profiles of (a) average liquid water content between 11:30 and 11:45 obtained from the remote sensing instruments and (b) cloud droplet effective radius (r_{eff}) for different cloud droplet number concentration profiles.